2464–2474 *Nucleic Acids Research, 2005, Vol. 33, No. 8*
doi:10.1093/nar/gki540

Studies on *Escherichia coli* RNase P RNA with Zn^{2+} as the catalytic cofactor

Simona Cuzic and Roland K. Hartmann*

Philipps-Universität Marburg, Institut für Pharmazeutische Chemie, Marbacher Weg 6, D-35037 Marburg, Germany

Received as resubmission February 18, 2005; Revised and Accepted April 11, 2005

ABSTRACT

We demonstrate, for the first time, catalysis by *Escherichia coli* ribonuclease P (RNase P) RNA with Zn^{2+} as the sole divalent metal ion cofactor in the presence of ammonium, but not sodium or potassium salts. Hill analysis suggests a role for two or more Zn^{2+} ions in catalysis. Whereas Zn^{2+} destabilizes substrate ground state binding to an extent that precludes reliable K_d determination, $Co(NH_3)_6^{3+}$ and Sr^{2+} in particular, both unable to support catalysis by themselves, promote high-substrate affinity. Zn^{2+} and $Co(NH_3)_6^{3+}$ substantially reduce the fraction of precursor tRNA molecules capable of binding to RNase P RNA. Stimulating and inhibitory effects of Sr^{2+} on the ribozyme reaction with Zn^{2+} as cofactor could be rationalized by a model involving two Sr^{2+} ions (or two classes of Sr^{2+} ions). Both ions improve substrate affinity in a cooperative manner, but one of the two inhibits substrate conversion in a non-competitive mode with respect to the substrate and the Zn^{2+}. A single 2′-fluoro modification at nt −1 of the substrate substantially weakened the inhibitory effect of Sr^{2+}. Our results demonstrate that the studies on RNase P RNA with metal cofactors other than Mg^{2+} entail complex effects on structural equilibria of ribozyme and substrate RNAs as well as E·S formation apart from the catalytic performance.

INTRODUCTION

The ribonucleoprotein enzyme ribonuclease P (RNase P) is an endonuclease that generates the mature 5′ ends of tRNAs in all three domains of life (Archaea, Bacteria and Eukarya) as well as in the mitochondria and the chloroplasts (1–3). Bacterial RNase P enzymes are composed of a catalytic RNA subunit, ~400 nt in length, and a single small protein of typically 120 amino acids (4,5). Studies with RNase P RNA from *Escherichia coli* (structural RNase P RNA subtype A) and *Bacillus subtilis* (subtype B) have implied a specific role for two or more metal ions in substrate binding and cleavage chemistry (6–13). Mg^{2+} and Mn^{2+} efficiently support the precursor tRNA (ptRNA) processing reaction catalyzed by bacterial RNase P RNAs (14), which generates 3′-OH and 5′-phosphate termini. For *E.coli* RNase P RNA (referred to as M1 RNA further), processing under standard assay conditions was reported to be essentially abolished when Mg^{2+} or Mn^{2+} is replaced with earth alkaline metals such as Sr^{2+}, transition metal ions, such as Zn^{2+}, Co^{2+} and Ni^{2+}, or $Co(NH_3)_6^{3+}$ as a potential mimic of hexaaquo Mg^{2+} (11,15). Ca^{2+}, as an exception, supported the reaction, although inefficiently (11,14). Different results were obtained with a ptRNA carrying an *R*p-phosphorothioate modification at the RNase P cleavage site. This substrate was cleaved quite efficiently by M1 RNA when Mg^{2+} was replaced with Cd^{2+}, conditions under which cleavage of the unmodified ptRNA was hardly detectable (7). This result suggested that the failure of transition metal ions such as Cd^{2+} to support cleavage of unmodified ptRNA by M1 RNA is due to their inability to interact properly with the phosphate *pro-R*p oxygen at the scissile phosphodiester in the transition state. The situation was found to be somewhat different in the reaction catalyzed by *B.subtilis* RNase P RNA. This ribozyme required a second metal ion, such as Ca^{2+}, in addition to Cd^{2+} for processing a ptRNA with a single *R*p-phosphorothioate modification at the cleavage site. Here, Ca^{2+} was inferred to be essential for productive enzyme–substrate complex formation (8), suggesting that there are differential roles for metal ions in RNase P RNA-catalyzed reactions. Synergistic effects of metal ion combinations were also observed for the reaction catalyzed by *E.coli* M1 RNA, although their molecular basis has been poorly understood. While the ribozyme failed to cleave the substrate in the presence of Ba^{2+}, Sr^{2+}, Zn^{2+} or $Co(NH_3)_6^{3+}$ alone, some cleavage activity was restored with the combinations Zn^{2+}/Sr^{2+}, Zn^{2+}/Ba^{2+} or $Zn^{2+}/Co(NH_3)_6^{3+}$ (11). Catalysis by M1 RNA with Sr^{2+} or Ba^{2+} alone has only been observed with low efficiency under very specialized conditions [at $pH \gg 7$ and in the presence of ethanol; (16)]. From the Pb^{2+}-induced hydrolysis patterns of M1 RNA generated in

*To whom correspondence should be addressed. Tel: +49 6421 28 25827; Fax: +49 6421 28 25854; Email: roland.hartmann@staff.uni-marburg.de

the presence of different divalent metal ions and $Co(NH_3)_6^{3+}$ (17), it was concluded that the M1 RNA conformation is very similar in the presence of Mg^{2+}, Mn^{2+}, Ca^{2+}, Sr^{2+}, Ba^{2+} and apparently also $Co(NH_3)_6^{3+}$, whereas transition metals, such as Zn^{2+} and particularly Cd^{2+}, Co^{2+}, Cu^{2+} and Ni^{2+}, induce changes of the native M1 RNA conformation.

To obtain a deeper insight into how different metal ions modulate this ribozyme system, we have investigated the effects of Zn^{2+}, Sr^{2+} and $Co(NH_3)_6^{3+}$ on different aspects of processing by M1 RNA: catalysis and its inhibition by Sr^{2+} in particular, enzyme–substrate affinity and changes in the fraction of substrate able to bind to the enzyme. Catalysis was analyzed under conditions of $E \gg S$, and all assays included a relatively high monovalent salt concentration (1 M NH_4OAc) to focus on the roles of metal ions which cannot be fulfilled by monovalent cations. To further characterize the metal ion interaction in vicinity of the 2′-OH group at nt −1 of the substrate, we have tested cleavage by M1 RNA in the presence of Zn^{2+}/Sr^{2+} with ptRNA substrates carrying a single 2′-amino (2′-N), 2′-fluoro (2′-F) or 2′-deoxy (2′-H) substitution at nt −1. Such 2′-ribose modifications at the RNase P cleavage site were previously reported to affect the binding of catalytically important Mg^{2+} and to substantially reduce the rate of catalysis by M1 RNA (6,18–20). Recent NMR experiments have provided further evidence that the metal ion coordinated with the help of the 2′-OH group at nt −1 is actually 'pre-bound' to ptRNA before complexation with RNase P RNA (21).

MATERIALS AND METHODS

RNA synthesis and labeling

Chemical and enzymatic RNA synthesis, purification of RNA and assembly of ptRNA variants with single-site modifications have been described recently (20).

Kinetics

Processing assays were performed at 37°C under single turnover conditions (5 μM M1 RNA, <1 nM ptRNA, 1 M NH_4OAc, 50 mM MES for the pH range of 5–6 and PIPES for pH 6–7; metal ion concentration and pH at 37°C as indicated) as described previously (22). Aliquots withdrawn from the enzyme–substrate mixtures were desalted by ethanol precipitation in the presence of 20 μg glycogen before analysis by 20% PAGE/8 M urea. Data analysis and calculation of single turnover rates of cleavage (k_{obs}) were performed as described previously (22).

The dependence of k_{obs} on $[Sr^{2+}]$ in Figure 7A and B showed a stimulatory and inhibitory phase. These primary data were replotted as k_{obs} in the absence of Sr^{2+} divided by k_{obs} at individual Sr^{2+} concentrations (termed v_0/v_i) over $[Sr^{2+}]$ (Figure 7C and D). These secondary plots were fit to the equation $v_0/v_i = (K_S + [E](1 + (1/\alpha K_{I(a)} + 1/\beta K_I)[I] + [I]^2/\alpha\beta K_{I(a)} K_I))/((K_S + [E])(1 + [I]/\alpha K_{I(a)}))$, derived from a model (Figure 8A) involving two Sr^{2+} ions (or two classes of Sr^{2+} ions): both improve substrate affinity in a cooperative manner, but one of the two inhibits substrate conversion in a non-competitive mode with respect to the substrate. The equation was derived as follows [E, M1 RNA; S, ptRNA substrate; I(a), Sr^{2+} with 'activating' effect owing to a reduction in K_S, expressed as $\alpha \cdot K_S$; I, inhibitory Sr^{2+} which also reduces K_S, expressed as $\beta \cdot K_S$].

The velocity dependence equation is:

$$v_i = k_{chem} \cdot ([ES] + [ESI(a)]). \quad \mathbf{1}$$

Dividing both sides of the velocity dependence Equation 1 by $[S]_t$:

$$\frac{v_i}{[S]_t} = \frac{k_{chem} \cdot ([ES] + [ESI(a)])}{[S]_t}. \quad \mathbf{2}$$

$$[S]_t = [S] + [ES] + [ESI] + [ESI(a)] + [ESI(a)I]. \quad \mathbf{3}$$

Replacing $[S]_t$ in the right-hand side of Equation 2:

$$\frac{v_i}{[S]_t} = \frac{k_{chem} \cdot ([ES] + [ESI(a)])}{[S] + [ES] + [ESI] + [ESI(a)] + [ESI(a)I]}. \quad \mathbf{4}$$

Expressing the concentration of each species in terms of [E]:

$$\frac{v_i}{[S]_t} = \frac{k_{chem} \cdot \left(\frac{[S]\cdot[E]}{K_S} + \frac{[S]\cdot[E]\cdot[I]}{\alpha\cdot K_S\cdot K_{I(a)}}\right)}{[S] + \frac{[S]\cdot[E]}{K_S} + \frac{[S]\cdot[E]\cdot[I]}{\beta\cdot K_S\cdot K_I} + \frac{[S]\cdot[E]\cdot[I]}{\alpha\cdot K_S\cdot K_{I(a)}} + \frac{[S]\cdot[E]\cdot[I]^2}{\alpha\cdot\beta\cdot K_S\cdot K_{I(a)}\cdot K_I}}. \quad \mathbf{5}$$

Multiplying the numerator and the denominator with $K_S/[S]$ and simplifying:

$$\frac{v_i}{[S]_t} = \frac{k_{chem}\cdot[E]\cdot\left(1 + \frac{1}{\alpha\cdot K_{I(a)}}\cdot[I]\right)}{K_S + [E]\cdot\left(1 + \left(\frac{1}{\beta\cdot K_I} + \frac{1}{\alpha\cdot K_{I(a)}}\right)\cdot[I] + \frac{1}{\alpha\cdot\beta\cdot K_I\cdot K_{I(a)}}\cdot[I]^2\right)}. \quad \mathbf{6}$$

When [I] = 0, v_i equals v_0, and Equation 6 simplifies to:

$$\frac{v_0}{[S]_t} = \frac{k_{chem}\cdot[E]}{K_S + [E]}. \quad \mathbf{7}$$

$[S]_t \cdot k_{chem}$ is V_{max} under conditions $[E] \gg [S]$.

Dividing Equation 7 by Equation 6 and simplifying:

$$\frac{v_0}{[S]_t} = \frac{K_S + [E]\cdot\left(1 + \left(\frac{1}{\beta\cdot K_I} + \frac{1}{\alpha\cdot K_{I(a)}}\right)\cdot[I] + \frac{1}{\alpha\cdot\beta\cdot K_I\cdot K_{I(a)}}\cdot[I]^2\right)}{(K_S + [E])\cdot\left(1 + \frac{1}{\alpha\cdot K_{I(a)}}\cdot[I]\right)}. \quad \mathbf{8}$$

Spin column assays

Spin column assays for the determination of equilibrium dissociation constants (K_d) of enzyme–substrate complexes were performed as described previously (8,23) in a buffer containing 50 mM MES, pH 6.0, 1 M NH_4OAc, 0.1% (w/v) SDS, 0.05% (w/v) Nonidet P-40, and indicated concentrations of $SrCl_2$, $Zn(OAc)_2$ and/or $Co(NH_3)_6Cl_3$. For the Hill plot analysis shown in Figure 3, see (9).

RESULTS

The well-characterized bacterial $ptRNA^{Gly}$ used as the substrate for processing by M1 RNA is illustrated in Figure 1, including the variants carrying single-site 2′-ribose modifications at nt −1.

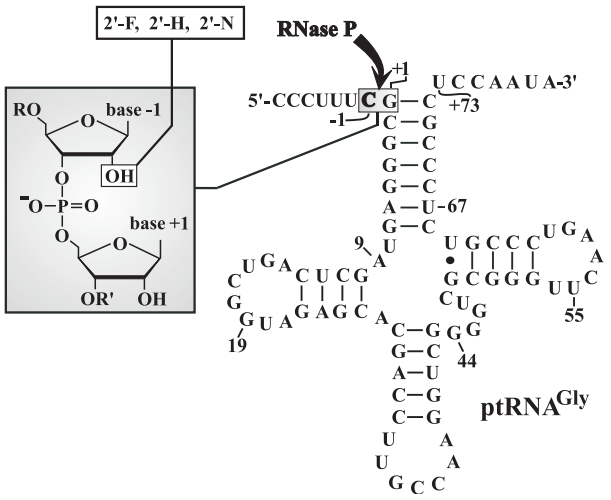

Figure 1. Secondary structure of the ptRNA^{Gly} substrate. 2′-Ribose modifications introduced at the canonical RNase P cleavage site (nt −1) are illustrated in the gray-shaded box on the left. The arrow marks the canonical RNase P cleavage site between nucleotides −1 and +1. For further details, see (20).

Cleavage in the presence of Zn^{2+} alone or combinations of Zn^{2+}/Sr^{2+} and $Zn^{2+}/Co(NH_3)_6^{3+}$

Surprisingly, Zn^{2+} as the only divalent metal ion was able to support ptRNA processing by M1 RNA, but only in the presence of ammonium salts (Figure 2A). The nature of the counter anion (chloride or acetate) was not critical (Figure 2A), although some RNA degradation was observed with chloride salts. Neither significant degradation nor precipitation of ptRNA or M1 RNA occurred under our standard assay conditions (1 M NH_4OAc, 20–80 mM $Zn[OAc]_2$, pH 6.65; data not shown). Sr^{2+} (Figure 2B) or $Co(NH_3)_6^{3+}$ (data not shown) alone did not support M1 RNA-catalyzed cleavage, in line with the previous observations (11).

We then analyzed single turnover cleavage by M1 RNA (see Materials and Methods) in the presence of Zn^{2+} and increasing concentrations of Sr^{2+} or $Co(NH_3)_6^{3+}$ (Figure 2C and D). The pH 6.65 was chosen to combine substantial substrate turnover with conditions where cleavage chemistry mainly determines the rate of cleavage at saturating enzyme concentrations (7). At constant 20 mM Zn^{2+}, both Sr^{2+} and $Co(NH_3)_6^{3+}$ started to stimulate substrate turnover at lower concentrations, followed by an inhibitory phase at higher concentrations (Figure 2C and D). This suggested that the two different Sr^{2+} or $Co(NH_3)_6^{3+}$ ions (or classes of ions) affected the cleavage reaction under these experimental conditions.

$Zn^{2+}/Sr^{2+}/Co(NH_3)_6^{3+}$ dependence of substrate binding to M1 RNA

As a next step, we analyzed the binding of ptRNA^{Gly} to M1 RNA as a function of Zn^{2+}, Sr^{2+} and/or $Co(NH_3)_6^{3+}$. The following results were obtained by a spin column assay (see Materials and Methods) and are summarized in Table 1. In the absence of any metal ion, a K_d of ~10 μM was measured under our assay conditions. The K_d increased to ⩾20 μM in the presence of 20 mM Zn^{2+}, demonstrating that the Zn^{2+} destabilizes the substrate ground state binding. Another transition metal ion, Cd^{2+}, supported E·S formation poorly as well (K_d of 2.1 μM), although more efficiently than the Zn^{2+}. In contrast to the transition metal ions, Sr^{2+} or $Co(NH_3)_6^{3+}$ support substrate binding, Sr^{2+} more efficiently than $Co(NH_3)_6^{3+}$. K_d values in the presence of 20 mM Zn^{2+} progressively decreased with increasing Sr^{2+} concentrations (Figure 3A). However, at all tested Sr^{2+} concentrations (5, 10, 20, 40 and 80 mM), the addition of 20 mM Zn^{2+} resulted in a constant 2–3-fold increase in K_d (Figure 3A). Moreover, the proportion of substrate that is able to form a stable complex with the enzyme at the endpoint (i.e. point of enzyme saturation; Figure 3A, numbers above bars) decreased with increasing ratios of [Zn^{2+}] to [Sr^{2+}], for example, the binding-proficient substrate fraction decreased from 0.92 at 20 mM Zn^{2+}/80 mM Sr^{2+} to 0.59 at 20 mM Zn^{2+}/5 mM Sr^{2+} (normalized to 1.0 measured at 40 mM Sr^{2+} alone, Figure 3A). Hill analysis of K_d in the presence of varying concentrations of Sr^{2+} and in the absence of Zn^{2+} gave a slope of n_H = 1.8 (Figure 3B), suggesting that at least two Sr^{2+} ions are additionally taken up into the enzyme–substrate complex under the applied conditions.

$Co(NH_3)_6^{3+}$ also decreased the K_d values, but the substrate affinity was lower relative to the equal concentrations of Sr^{2+} (Table 1), suggesting that $Co(NH_3)_6^{3+}$ is a rather inefficient substitute for hexahydrated Mg^{2+} in this system. Whereas K_d values in the presence of Sr^{2+} were generally increased by the addition of 20 mM Zn^{2+} (Figure 3A), addition of 20 mM Zn^{2+} to 20 or 80 mM $Co(NH_3)_6^{3+}$ tended to lower K_d to some extent compared with the corresponding $Co(NH_3)_6^{3+}$ alone conditions (Table 1). This suggests that Zn^{2+} and $Co(NH_3)_6^{3+}$ weakly complement each other in promoting E·S complex formation. Remarkably, higher concentrations (e.g. 80 mM) of $Co(NH_3)_6^{3+}$ substantially lowered the proportion of ptRNA capable of complex formation under saturating enzyme concentrations [0.26 for 80 mM $Co(NH_3)_6^{3+}$ versus 0.98 for 80 mM Sr^{2+}; Table 1].

Zn^{2+} cooperativity in catalysis by M1 RNA

We observed that M1 RNA is able to catalyze ptRNA processing in the presence of Zn^{2+} as the sole divalent metal ion (Figure 2A). On the other hand, Zn^{2+} failed to promote thermodynamically stable E·S complex formation (Table 1 and Figure 3A), in contrast to other divalent metal ions, such as Mg^{2+} or Mn^{2+}, which support both catalysis and E·S formation (14). Thus, processing analyses with Zn^{2+} suggested the potential to use Zn^{2+} as a specific tool to study catalysis apart from E·S complex formation.

To assess the number of catalytic Zn^{2+} ions involved, we analyzed single turnover cleavage of ptRNA^{Gly} in the presence of increasing Zn^{2+} concentrations, either in the presence of constant 12 mM Sr^{2+} or 20 mM $Co(NH_3)_6^{3+}$, or without any second metal ion (Figure 4). For the conditions including Sr^{2+} and $Co(NH_3)_6^{3+}$, enzyme concentration (5 μM) was saturated based on our K_d measurements (Table 1 and Figure 3A). In all cases, reasonable fits to the Hill equation resulted in coefficients of n_H = 2.2 (Figure 4A, at constant 12 mM Sr^{2+}), n_H = 2.8 (Figure 4B, Zn^{2+} alone) and n_H = 1.8 [Figure 4C, at constant 20 mM $Co(NH_3)_6^{3+}$]. These n_H-values in the range 1.8–2.8 support the cooperative involvement of two or more Zn^{2+} ions in catalysis by *E.coli* M1 RNA. Results from the

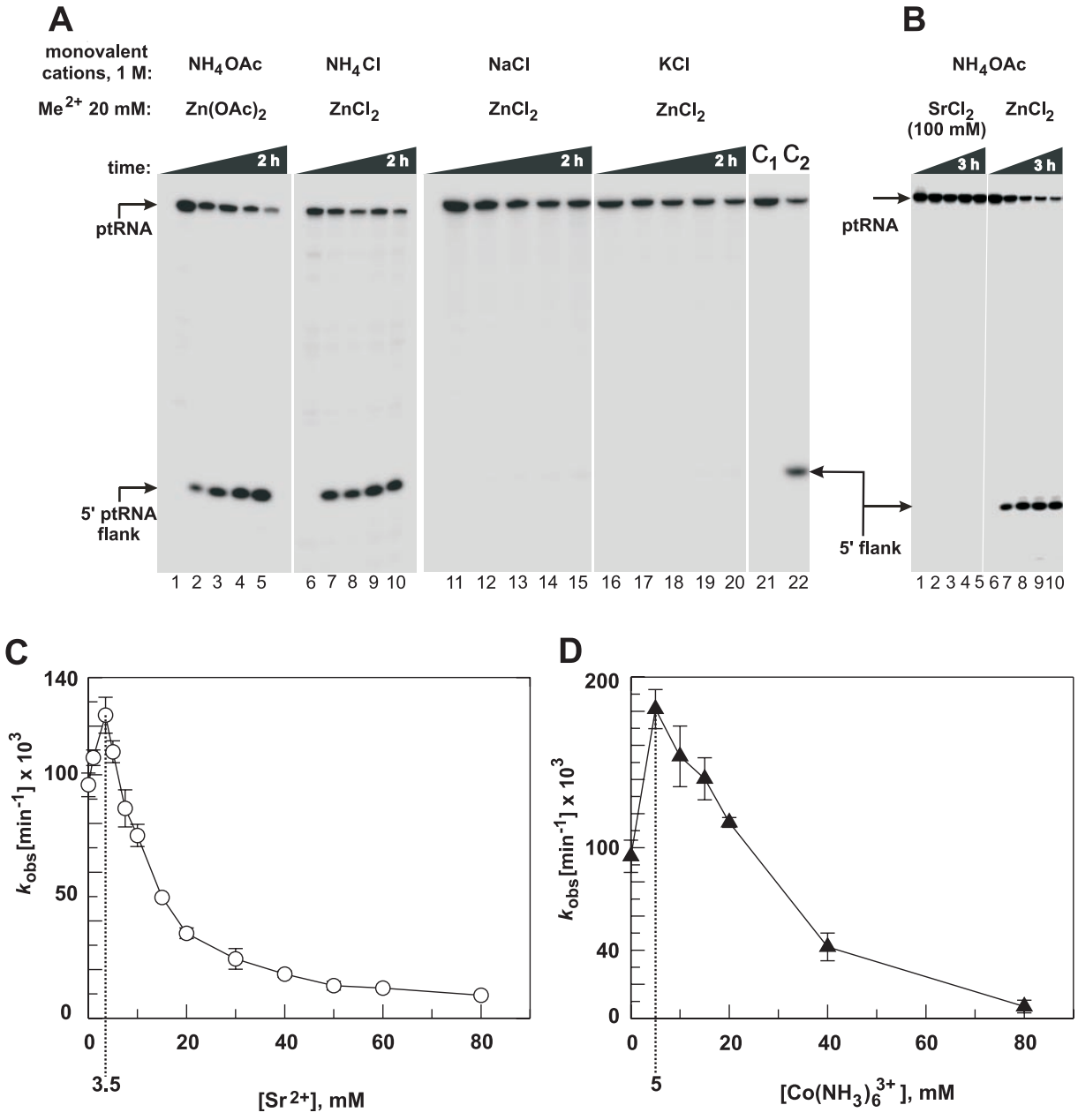

Figure 2. Processing of the all-ribose ptRNA^{Gly} by *E.coli* M1 RNA under single turnover conditions at 37°C in the presence of 20 mM Zn^{2+}. (**A**) Dependence on the type of monovalent cation; processing occurred in the presence of ammonium, but not sodium or potassium salts; reaction conditions: 5 μM M1 RNA, <1 nM ptRNA, 50 mM PIPES, pH 6.65, 1 M monovalent salt as indicated, and 20 mM $ZnCl_2$ or $Zn(OAc)_2$; control lanes 1, 6, 11, 16 and 21: incubation for 2 h in the absence of M1 RNA; time points were 5 min (lanes 2, 7, 12, 17 and 22), 20 min (lanes 3, 8, 13 and 18), 1 h (lanes 4, 9, 14 and 19) and 2 h (lanes 5, 10, 15 and 20); lanes 21 and 22 (C_1, C_2) are equal to lanes 1 and 2. (**B**) Assay documenting that no processing occurs in the presence of Sr^{2+} as the sole metal ion; reaction conditions: 5 μM M1 RNA, <1 nM ptRNA, 50 mM PIPES, pH 6.65, 1 M NH_4OAc and 100 mM $SrCl_2$ (left) or 20 mM $ZnCl_2$ (right). Control lanes 1 and 6: incubation for 3 h in the absence of M1 RNA; time points were 5 min (lane 7), 20 min (lanes 2 and 8), 40 min (lane 3), 1 h (lanes 4 and 9) and 3 h (lanes 5 and 10). (**C** and **D**) Processing rates as a function of increasing concentrations of $SrCl_2$ (C) or $Co(NH_3)_6Cl_3$ (D); reaction conditions: 5 μM M1 RNA, <1 nM ptRNA, 50 mM PIPES, pH 6.65, 1 M NH_4OAc and 20 mM $Zn(OAc)_2$; transition points between the stimulatory and the inhibitory phases of the curves are marked by dashed lines.

Zn^{2+}-alone reaction, although supporting this Zn^{2+} cooperativity, should yet be interpreted with some caution as the enzyme concentration was subsaturating under these conditions (Table 1); thus, we cannot exclude that, in addition to the rate of the catalytic step, changes in the E·S binding equilibrium upon variation of [Zn^{2+}] may also have affected the observed cleavage rates.

Processing of substrates with 2′-ribose modifications at nt −1 in the presence of Zn^{2+}/Sr^{2+}

A model of the RNase P RNA cleavage mechanism [(24); Figure 5, model I] proposes that one Mg^{2+} ion (termed here Mg[B]) simultaneously interacts with the OH^- nucleophile (inner-sphere) and the 2′-OH at position −1 of the substrate

Table 1. Influence of Zn^{2+}, Sr^{2+} and/or $Co(NH_3)_6^{3+}$ on the binding of $ptRNA^{Gly}$ to *E.coli* M1 RNA

Metal ion(s) Transition Me^{2+}	Other	K_d (nM)	Average endpoint
—	—	10 000 ± 3000	0.66
20 mM Zn^{2+}	—	⩾20 000[a]	n.d.[a]
20 mM Cd^{2+}	—	2100 ± 400	0.75
—	5 mM Sr^{2+}	240 ± 15	0.93
20 mM Zn^{2+}	5 mM Sr^{2+}	700 ± 300	0.59
—	80 mM Sr^{2+}	4 ± 0.5	0.98
20 mM Zn^{2+}	80 mM Sr^{2+}	9 ± 0.5	0.92
20 mM Zn^{2+}	5 mM $Co(NH_3)_6^{3+}$	2486 ± 400	0.55
—	20 mM $Co(NH_3)_6^{3+}$	751 ± 200	0.75
20 mM Zn^{2+}	20 mM $Co(NH_3)_6^{3+}$	350 ± 120	0.65
—	80 mM $Co(NH_3)_6^{3+}$	79 ± 35	0.26
20 mM Zn^{2+}	80 mM $Co(NH_3)_6^{3+}$	53 ± 6	0.28

Spin column assay for the determination of K_d values were performed at pH 6.0 and 1 M NH_4OAc using trace amounts of 5′-endlabeled $ptRNA^{Gly}$; individual K_d values are based on three to six independent experiments and were calculated by non-linear regression analysis (program Grafit, Erithacus Software) using the equation: $f_c = f_t \cdot [\text{P RNA}]_{free}/(K_d + [\text{P RNA}]_{free})$, where f_c = fraction of ptRNA in the complex, and f_t = maximum fraction of ptRNA that is able to bind to P RNA (endpoint). Endpoints in the right column are the theoretical ones obtained by the fitting procedure; however, theoretical and experimentally measured endpoints were generally in good agreement; average endpoints were normalized to that for 40 mM Sr^{2+} (see Figure 3A).

[a]K_d and endpoint values (n.d. = not determined) could not be determined with reasonably low errors owing to very low ribozyme–substrate affinity; the K_d of 20 000 nM in the presence of 20 mM Zn^{2+} alone is a lower limit estimate.

via an inner-sphere water molecule, and directly coordinates to the *pro-R*p phosphate oxygen at the cleavage site. In an alternative model (Figure 5, model II), two metal ions (Mg[A] and Mg[B]) directly coordinate to the *pro-R*p oxygen, but Mg[A] instead of Mg[B] interacts with the OH^- nucleophile via inner-sphere coordination (7,25). In both models, Mg[B] interacts with the 2′-OH function at nt −1 of the substrate via an inner-sphere water molecule.

We addressed the possibility that Sr^{2+} may displace catalytically important Zn^{2+} at the aforementioned metal ion binding site [B], assuming that the binding sites for the two different metal ions overlap to such an extent that their binding is mutually exclusive. We have recently shown that 2′-substitutions at nt −1 of ptRNA decreased cleavage efficiency by M1 RNA in the order 2′-H ⩽ 2′-N < 2′-F < 2′-OH under conditions of rate-limiting chemistry (20). Assuming that Sr^{2+} indeed displaces a Zn^{2+} ion that is bound to site [B] involving the 2′-OH at nt −1 of ptRNA (Figure 5), one would expect that these 2′-modifications change the affinities of Zn^{2+} and Sr^{2+} (which largely differ in their electronic properties and the details of their coordination spheres; see Discussion) to different extents. In contrast, the competition profile should be much less affected if Sr^{2+} displaces catalytic Zn^{2+} at a site other than [B], where metal ion coordination is not directly dependent on the 2′-OH at nt −1. In fact, the concentration of Sr^{2+} at the transition point between the stimulatory and the inhibitory phases of the curve was substantially shifted toward higher Sr^{2+} concentrations (20–40 mM versus 3.5 mM, Figure 6A) when the 2′-OH at nt −1 was replaced with a 2′-F, 2′-N or 2′-H substituent. We then tested if this shift in the inflection point of the curve is a specific feature associated with the 2′-ribose modifications at nt −1 rather than a general effect, for example, related to a reduction in the rate of the chemical step (k_{chem}). We, therefore, analyzed the Sr^{2+} dependence of cleavage rate for the all-ribose substrate at two lower pH values to reduce the rate of k_{chem}. The inflection point of the curve indeed increased with decreasing pH (Figure 6B), which also holds for cleavage of the 2′-F-ptRNA measured at the same three pH values (Figure 6C). These findings suggested that it may be difficult to extract metal ion-specific information based on changes of the inflection point between the stimulatory and the inhibitory phases.

Our affinity measurements (Figure 3A and Table 1) showed that an enzyme concentration of 5 μM was subsaturating at 20 mM Zn^{2+} and ≪ 5 mM Sr^{2+}. Since we attributed the stimulatory effect of Sr^{2+} at low concentrations to its stabilization of E·S complexes, we suspected that changes in [E] may also affect the inflection point between the stimulatory and the inhibitory phases. Indeed, the Sr^{2+}-dependence of processing rate displayed changes in the inflection point between the two phases for the all-ribose as well as the 2′-F-ptRNA when monitored at enzyme concentrations of 5 versus 1.4 μM (Figure 7A and B). We then replotted the data of Figure 7A and B as v_0/v_i (v_0 and v_i correspond to k_{obs} in the absence and the presence of Sr^{2+}, respectively; Figure 7C and D). The best fit of the data was obtained utilizing Equation 8 (see Materials and Methods) based on a model outlined in Figure 8A, which involves two Sr^{2+} ions (or two classes of Sr^{2+} ions); both ions improve substrate affinity in a cooperative manner, but one of the two inhibits substrate conversion in a non-competitive mode with respect to the substrate. The two Sr^{2+} ions may well be those suggested by the Hill coefficient of the binding data in Figure 3B. The fact that both Sr^{2+} ions contribute to the formation of high-affinity E·S complexes is accounted for by introducing the interaction factors α and β in the scheme of Figure 8A. Other models, for example, assuming the involvement of two 'activating' and one inhibitory Sr^{2+} ion or predicting that E·S·I and E·S·I(a)·I complexes retain residual reactivity, failed to give satisfactory curve fits of the data.

Mode of inhibition by Sr^{2+}

We finally investigated the inhibition mode of Sr^{2+} with respect to the Zn^{2+} by varying the Sr^{2+} concentration between 10 and 40 mM at four different Zn^{2+} concentrations. Under these conditions, the enzyme concentration (5 μM) was assumed to be saturating at all variations of Sr^{2+} and Zn^{2+}, even at the combination of 10 mM Sr^{2+} and 20 mM Zn^{2+},

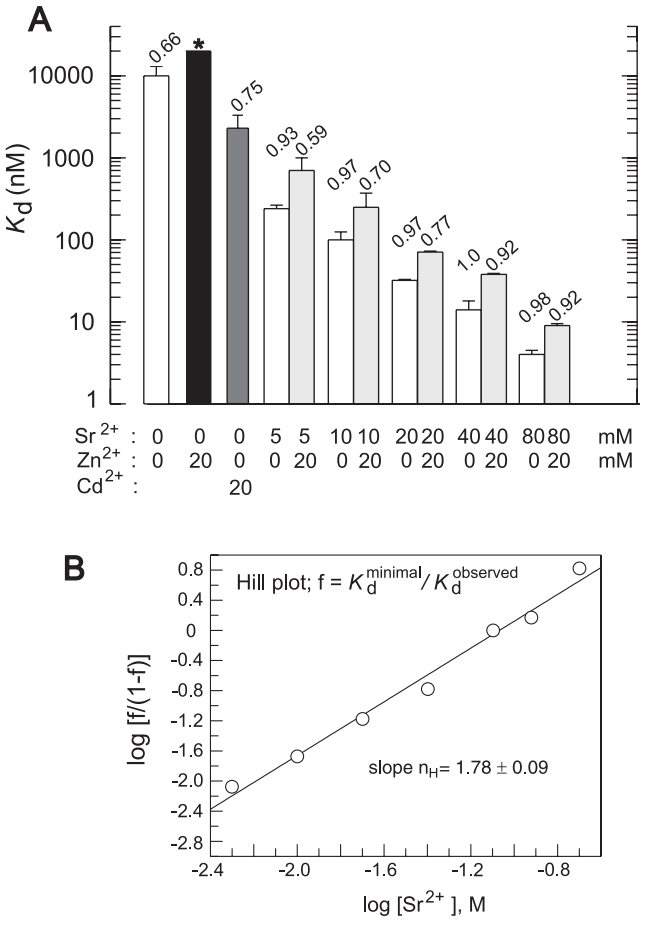

Figure 3. K_d values for ptRNA^{Gly} binding to M1 RNA determined by the spin column assay (8,23). Assay buffers contained 50 mM MES, pH 6.0, 1 M NH_4OAc and indicated concentrations of Sr^{2+} and/or Zn^{2+}. (**A**) Bar diagram of log K_d dependence on Sr^{2+} and/or Zn^{2+} (or Cd^{2+}) concentration as indicated below the diagram. Values above bars represent the proportion of ptRNA^{Gly} that was able to form a complex with M1 RNA at the theoretical endpoint (M1 RNA saturation), normalized to conditions of 40 mM Sr^{2+}. Asterisk above the black bar for conditions of 20 mM Zn^{2+} alone: the experimental endpoint could not be reached due to very weak complex formation, which resulted in high errors for K_d determinations; the K_d of ⩾20 μM is therefore only an estimate. Individual values are based on average on four independent experiments; errors are indicated by error bars. (**B**) Hill plot analysis of K_d dependence on Sr^{2+} concentration. f = (minimal K_d)/(observed K_d); the minimal K_d at saturating Sr^{2+} concentrations was determined as 2 nM.

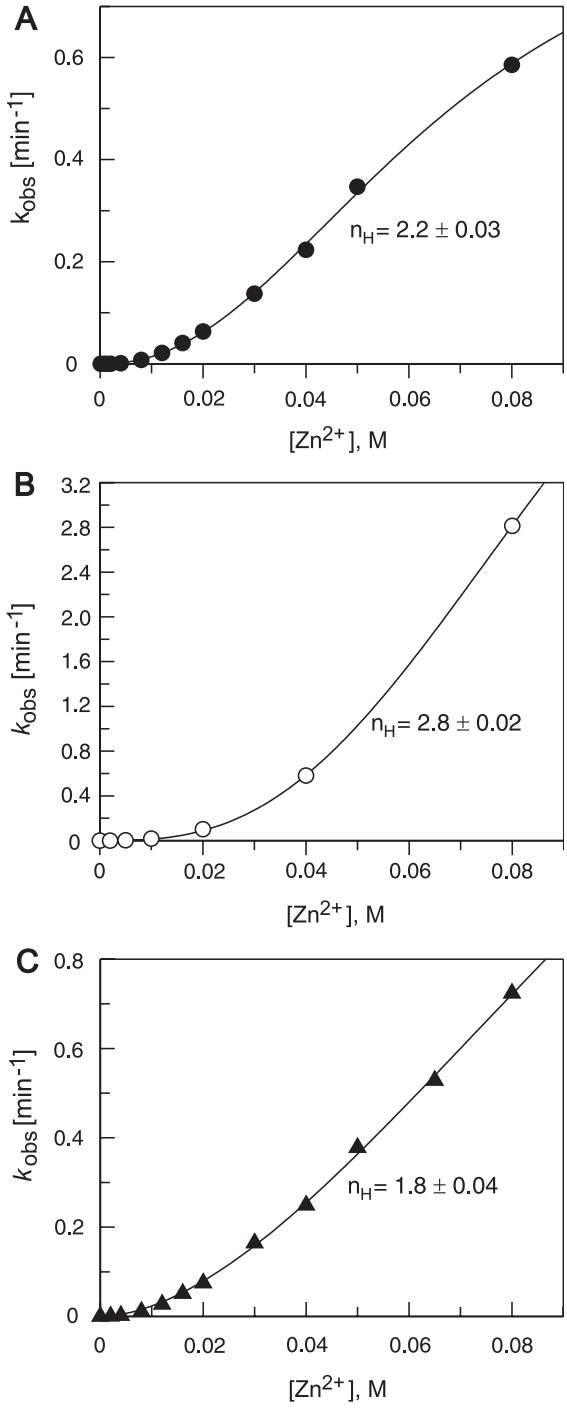

Figure 4. Zn^{2+}-dependence of M1 RNA-catalyzed cleavage of all-ribose ptRNA^{Gly} (Hill analysis). The Zn^{2+}-concentration was varied in the range of 0–80 mM: (**A**) at constant [Sr^{2+}] (12 mM) and pH 6.0; (**B**) in the absence of a second metal ion at pH 6.5; (**C**) at constant [$Co(NH_3)_6^{3+}$] (20 mM) and pH 6.0. Data were analyzed by non-linear regression analysis using the Hill equation $v = V_{max}\cdot[Zn^{2+}]^n/(K'_{Zn} + [Zn^{2+}]^n)$ as described previously (8). The Hill coefficient (n_H) was determined as 2.2 ± 0.03 in (A), 2.8 ± 0.02 in (B) and 1.80 ± 0.04 in (C). For further details, see Materials and Methods.

where a K_d of ∼250 nM was determined (Figure 3A). Thus, cleavage chemistry was expected to limit the rate of substrate turnover. The Dixon plot of the data (Figure 8B) gave straight lines that intersect on the [I] axis, which is a specific feature of non-competitive inhibition. The point of intersection yields a K_I value of ∼5 mM. The result argues against a direct displacement of catalytic Zn^{2+} by a Sr^{2+} ion at the aforementioned metal ion site [B] (Figure 5).

DISCUSSION

Catalysis in the presence of Zn^{2+}

M1 RNA-catalyzed processing in the presence of Zn^{2+} as the only divalent metal ion present in the cleavage assay (termed Zn^{2+} alone conditions in the following) is in contrast to the previous studies (11,15). This discrepancy can be explained by the fact that our study was performed under conditions of E ≫ S and in the presence of high concentrations of NH_4OAc. With potassium or sodium instead of ammonium salts, we

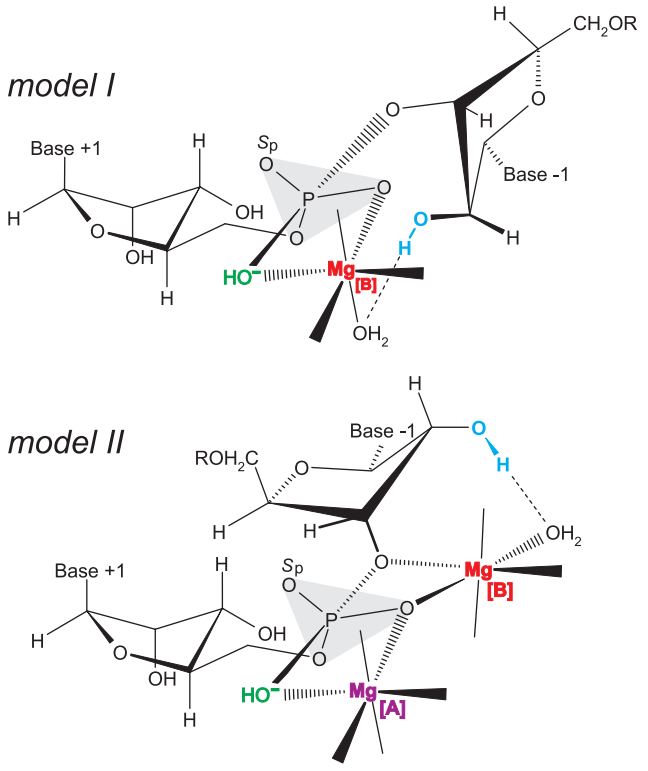

Figure 5. Transition state models for phosphodiester hydrolysis by *E.coli* M1 RNA. The single 2′-OH at nt −1 (in blue) was replaced with a 2′-deoxy, 2′-amino or 2′-fluoro group in the modified substrates analyzed in Figure 6. Putative, catalytically important Mg^{2+} ions are shown in magenta (Mg [A]) or red (Mg [B]); metal ion site [B] was in the focus of the present study. The first transition state model (model I) for hydrolysis of the scissile phosphodiester connecting nt +1 and −1 is derived from that proposed in (24), according to which the Mg^{2+} ion at the site termed [B] here directly coordinates to the *pro-R*p phosphate oxygen and OH^- nucleophile (in green), and simultaneously interacts with the 2′-OH at position −1 via an inner-sphere water molecule. According to model II, two Mg^{2+} ions, Mg[A] and Mg[B], directly coordinate to the *pro-R*p oxygen (7,25), but Mg[A] instead of Mg[B] interacts with the OH^- nucleophile via inner-sphere coordination. Additional metal ion interactions at the *pro-S*p oxygen (marked Sp; models I and II) and the 3′-bridging oxygen (model I) are conceivable based on strong inhibition effects caused by sulfur substitutions at these positions (7,24,35). The ribose at nt +1 are drawn in the A-helical C3′-*endo* and the ribose at position −1 in the C2′-*endo* conformation based on the results of NMR investigations (36,37).

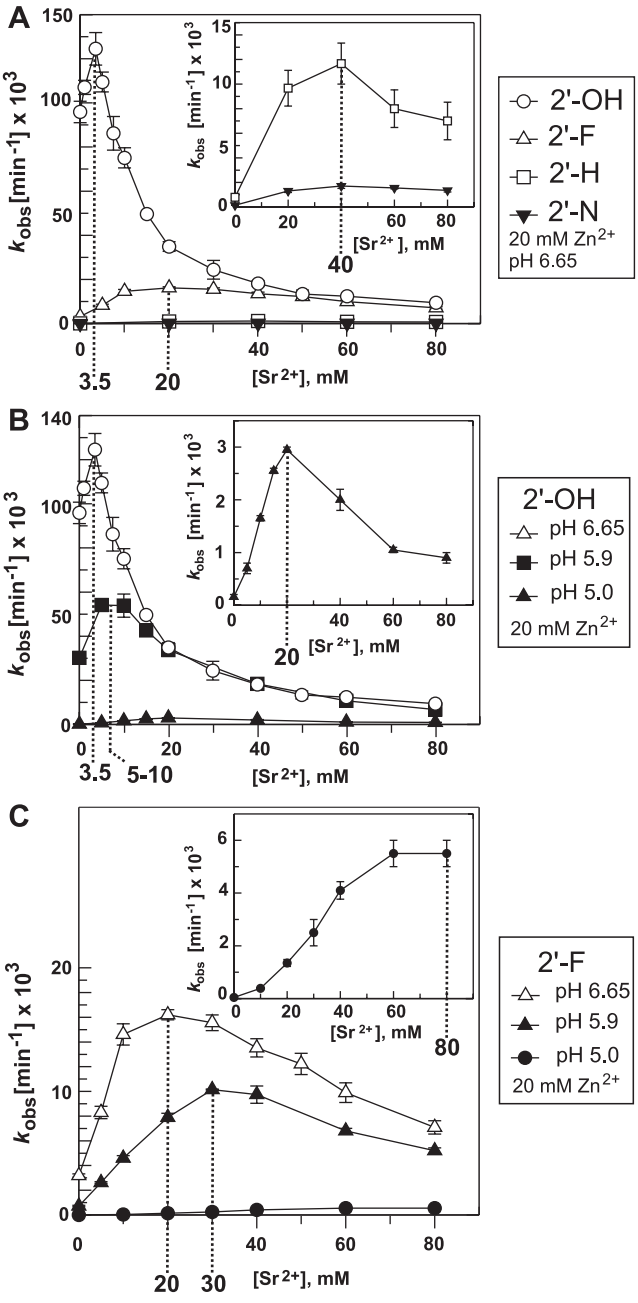

Figure 6. Processing by M1 RNA of the all-ribose ptRNA^{Gly} (2′-OH) and variants thereof with a single 2′-fluoro (2′-F), 2′-deoxy (2′-H) or 2′-amino (2′-N) modification at nt −1. (**A**) Processing rates in the presence of 20 mM Zn^{2+} and varying concentrations of Sr^{2+} at pH 6.65. Inflection points between stimulatory and inhibitory phases of curves are marked by dashed lines. The curve for the all-ribose ptRNA^{Gly} is identical to that shown in Figure 2C. The inset shows the curves for the 2′-H- and 2′-N-modified substrates at higher resolution. (**B**) Processing rates for all-ribose ptRNA^{Gly} at three different pH values. (**C**) As in (B), but using the 2′-F-modified ptRNA^{Gly}. For further details, see Materials and Methods.

were unable to detect M1 RNA-catalyzed cleavage under Zn^{2+}-alone conditions (Figure 2A). One possibility is that Zn^{2+} ions partly replace water ligands with ammonia (26) as a requirement to be able to sustain catalysis by M1 RNA. Although proficient in catalysis, Zn^{2+} is unable to support thermodynamically stable E·S complex formation (Table 1 and Figure 3A). Yet selection of the canonical cleavage site (between nt −1 and +1) was not changed in the presence of Zn^{2+} alone (relative to Mg^{2+} alone; data not shown), despite the very low substrate affinity under Zn^{2+} alone conditions. This shows that low affinity substrate ground state binding not necessarily favors aberrant cleavage (between nt −2 and −1) relative to cleavage at the canonical site. One interpretation is that the high activation barrier difference for aberrant cleavage (at −2/−1) relative to canonical cleavage (−1/+1) is maintained under these conditions. In conclusion, RNase P RNA catalysis with Zn^{2+} as the metal cofactor represents a ribozyme case where the specific transition state is achieved despite a dramatic destabilization of the substrate ground state binding.

We had speculated that the inability of Zn^{2+} to mediate high-affinity substrate binding might enable us to dissect the metal ions that mediate substrate ground state binding from

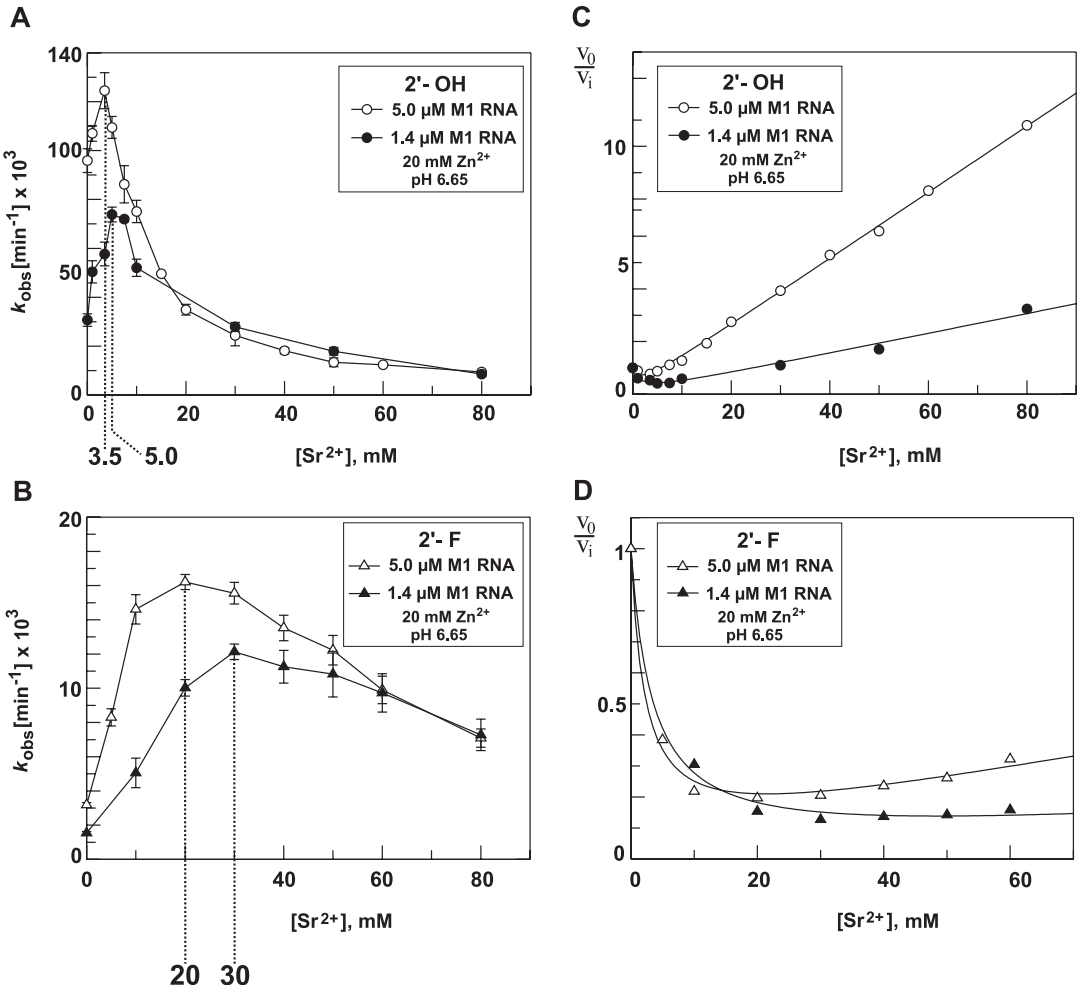

Figure 7. Sensitivity of processing rates as a function of $[Sr^{2+}]$ to differences in [E]: (**A**) all-ribose ptRNA^{Gly} (2′-OH); (**B**) 2′-F-ptRNA^{Gly}. (**C** and **D**) Secondary v_0/v_i plots of the data ($v_0 = k_{obs}$ in the absence of Sr^{2+}; $v_i = k_{obs}$ at the respective Sr^{2+} concentration) from (A) and (B). Data fitting was best with the model depicted in Figure 8A, using Equation 8 (see Materials and Methods and Figure 8): $v_0/v_i = (K_S + [E]\,(1 + (1/\alpha K_{I(a)} + 1/\beta K_I)\,[I] + [I]^2/\alpha\beta K_{I(a)}\,K_I))/((K_S + [E])\,(1 + [I]/\alpha K_{I(a)}))$. Curve fits yielded the following values for $\alpha K_{I(a)}$ and βK_I: 1.46 ± 0.46 mM and 0.72 ± 0.025 mM [(C), 1.4 μM M1 RNA, 2′-OH], 1.49 ± 0.45 mM and 0.72 ± 0.005 mM [(C) 5 μM M1 RNA, 2′-OH], 3.5 ± 0.4 and 9.1 ± 2.1 mM [(D) 1.4 μM M1 RNA, 2′-F] and 2.2 ± 0.2 and 11 ± 0.8 mM [(D) 5 μM M1 RNA, 2′-F]; estimates for K_S were 50 and 120 μM in (C) and (D), respectively.

those specifically involved in transition state stabilization in order to define the subset of catalytic metal ions. This, however, turned out to be difficult because saturating enzyme concentrations could not be reached in the absence of a second non-catalytic metal ion, such as Sr^{2+}, but Sr^{2+} in turn [as $Co(NH_3)_6^{3+}$] inhibited catalysis. This resulted in complex velocity versus $[Sr^{2+}]$ curves with ascending and descending sections (Figure 2C, 6, 7A and B). Secondary plots of these data gave reasonable fits to a model involving two Sr^{2+} ions (or two classes of Sr^{2+} ions). Both Sr^{2+} ions support substrate binding in a cooperative manner, but one of the two inhibits substrate conversion. In a non-competitive mode with respect to the substrate. As a result, Sr^{2+} stimulated processing at low concentrations by shifting the E·S equilibrium toward complex formation, whereas the inhibitory effect dominated at higher concentrations. Curves of k_{obs} versus $[Sr^{2+}]$ turned out to be highly sensitive to changes in [E] or k_{chem} (Figures 6 and 7). By analyzing Sr^{2+} inhibition of M1 RNA-cleavage with Zn^{2+} as catalytic cofactor in the context of different substrates with 2′-ribose modifications, we had hoped to extract specific information regarding the catalytic metal ion binding to site [B] (Figure 5). Indeed, the βK_I values for Sr^{2+} inhibition derived from the secondary plots in Figure 7C and D are ∼15-fold higher for the 2′-F versus all-ribose ptRNA substrate, while $\alpha K_{I(a)}$ values are equal within a factor of 2. This finding is consistent with the binding of an Sr^{2+} ion at or near metal ion site [B] with the help of the 2′-OH at nt −1. However, inhibition kinetics (Figure 8B) with the all-ribose substrate favored a model of non-competitive inhibition of Sr^{2+} with respect to Zn^{2+}, thus arguing against a mechanism in which the inhibitory Sr^{2+} ion directly displaces a catalytic Zn^{2+} at metal ion site [B]. It, therefore, remains to be defined how Sr^{2+} inhibits the catalytic process with Zn^{2+} as catalytic cofactor.

Our kinetic analyses (Figure 4) have revealed an involvement of two or more Zn^{2+} ions, or classes of Zn^{2+} binding sites, in M1 RNA catalysis. This result is similar to those obtained with Mg^{2+} as the metal ion cofactor (6). These authors concluded that at least three Mg^{2+} ions take part in the catalytic step.

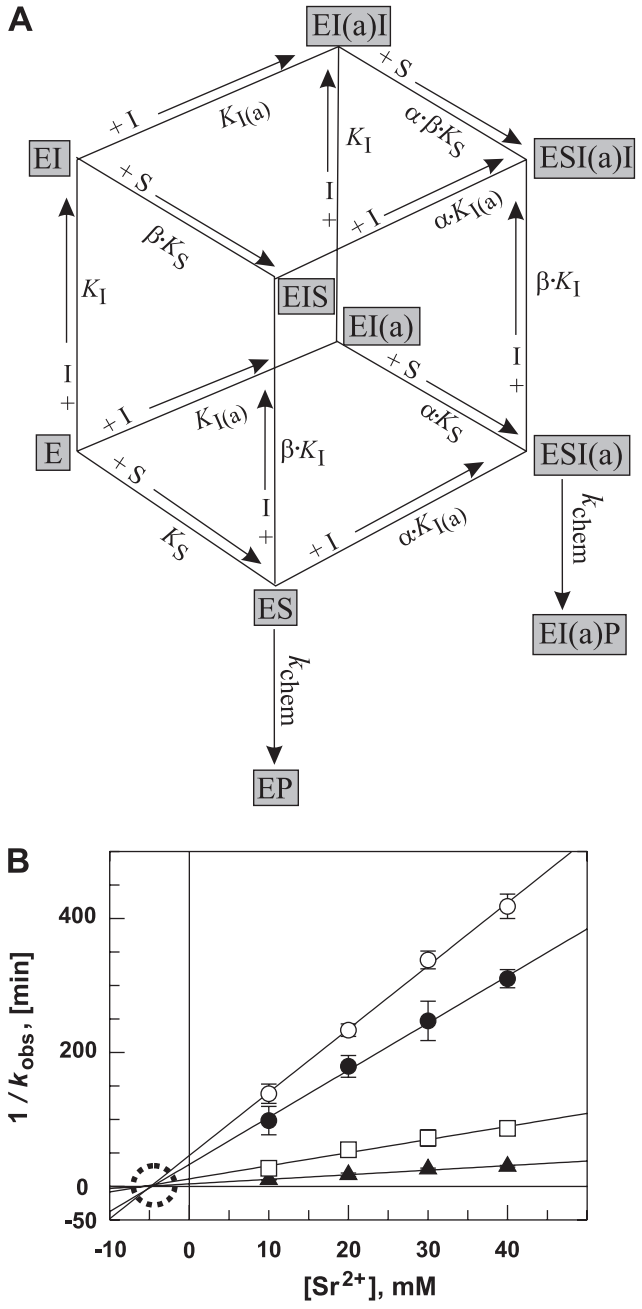

Figure 8. (**A**) Equilibria for the M1 RNA-catalyzed processing reaction in the presence of constant $[Zn^{2+}]$ as the catalytic cofactor and varying concentrations of $[Sr^{2+}]$ that activate the reaction at low but inhibit at higher concentrations. The model involves two Sr^{2+} ions (or two classes of Sr^{2+} ions) that both improve substrate affinity in a cooperative manner (see Figure 3B), but one of the two inhibiting substrate conversion non-competitively with respect to the substrate. Other models, for example, assuming the involvement of two 'activating' and one inhibitory Sr^{2+} ion or predicting that E·S·I and E·S·I(a)·I complexes retain residual reactivity, failed to give satisfactory curve fits of the data in Figure 7C and D. I(a) = Sr^{2+} ion that activates processing by decreasing K_S to αK_S; I = inhibitory Sr^{2+} ion that inhibits cleavage chemistry but also decreases K_S to βK_S. (**B**) Dixon plot of the M1 RNA-catalyzed ptRNA cleavage rate at 37°C as a function of $[Sr^{2+}]$ in the presence of four different fixed Zn^{2+} concentrations and 5 μM M1 RNA, <1 nM ptRNA, 50 mM PIPES, pH 6.65 and 1 M NH_4OAc; open circles, 8.1 mM Zn^{2+}; filled circles, 10 mM Zn^{2+}; open squares, 15 mM Zn^{2+}; and filled triangles, 20 mM Zn^{2+}. All four datasets fit to straight lines intersecting on the *x*-axis, indicating that Sr^{2+} acts as a non-competitive inhibitor with respect to Zn^{2+}. The point of intersection on the *x*-axis yields a K_I-value of ~5 mM.

Zn^{2+} has also been explored as a catalytic cofactor in the reaction catalyzed by the *B.subtilis* holoenzyme (9) with an RNA subunit of the structural type B. Single turnover activity (with 1 μM holoenzyme and 100 mM KCl, pH 8.0) was very low in the presence of 10 mM Zn^{2+} (2.4×10^{-3} min^{-1}). However, the addition of 2 mM $Co(NH_3)_6^{3+}$ in combination with only 0.2 mM Zn^{2+} resulted in a processing rate of ~11 min^{-1}, which was only ~5-fold lower than the cleavage rate under saturating Mg^{2+} conditions, with Zn^{2+} activating cleavage at lower concentrations than Mg^{2+} (9). The latter is attributable to the fact that Zn^{2+} (as Mn^{2+}) is a better Lewis acid than Mg^{2+} [pK_a for the formation of $Me[H_2O]_5[OH]^+$ of ~9.0 versus 11.4 for Mg^{2+}; (27)]. These results combined with ours obtained for the *E.coli* system document that Zn^{2+} is a proficient cofactor of bacterial RNase P (RNA) catalysis.

Comparison with results from the previous studies of M1 RNA

The global conformation of M1 RNA has previously been probed by lead ion-induced hydrolysis in the absence of substrate (17). Cd^{2+} substantially altered the lead hydrolysis pattern of M1 RNA relative to Mg^{2+}, while changes were more moderate in the presence of Zn^{2+}, which suggested substantial changes of M1 conformation induced by Cd^{2+} but to a lower extent by Zn^{2+} (17). These findings are entirely different from the relative effects of Zn^{2+} and Cd^{2+} on the substrate affinity observed in the work presented here, indicating that Zn^{2+} is much more detrimental to E·S formation than Cd^{2+} at the same concentrations (Table 1). Yet, despite the better performance of Cd^{2+} in E·S formation, Zn^{2+} supports cleavage of the all-ribose ptRNA at a 16-fold higher rate than Cd^{2+} (data not shown) under our standard conditions (Figure 2A, in the presence of 1 M NH_4OAc and 20 mM Me^{2+}). This may be related to the fact that the formation of an $Me[H_2O]_5[OH]^+$ species required for RNase P catalysis (see below) is favored with Zn^{2+} over Cd^{2+} [pK_a of ~9.0 for Zn^{2+} versus >10 for Cd^{2+}; (27)].

The lead-induced hydrolysis patterns of M1 RNA also suggested that the M1 RNA conformation is rather similar in the presence of Mg^{2+}, Mn^{2+}, Ca^{2+}, Sr^{2+}, Ba^{2+} and $Co(NH_3)_6^{3+}$ (17). However, we found that $Co(NH_3)_6^{3+}$ at higher concentrations substantially reduced the fraction of ptRNA substrates capable of binding to saturating concentrations of M1 RNA, which was also observed to some extent for Zn^{2+} (Table 1 and Figure 3A). Likewise, Zn^{2+} and $Co(NH_3)_6^{3+}$ are expected to affect the proportion of catalytically competent M1 RNA, which will be of particular importance when cleavage assays are performed in the presence of limited amounts of ribozyme (E ≪ S). In conclusion, future studies will have to incorporate the differential effects that metal ions (or metal ion mimics) other than Mg^{2+} have on structural equilibria of ribozyme and substrate RNAs as well as E·S complex formation in addition to the catalytic performance.

Failure of Sr^{2+} to support catalysis

Little is known on the binding of Sr^{2+} ions to RNA, but a coordination geometry different from the canonical octahedral Mg^{2+} geometry may be the cause for the failure of Sr^{2+} to activate catalysis by RNase P RNA under standard conditions and its inhibitory mode in the reaction with Zn^{2+} as the metal

cofactor. Indeed, a coordination geometry resembling a slightly distorted trigonal prism and involving nine oxygen atoms (four ribose hydroxyl groups and five waters) were observed for a Sr^{2+} ion in the crystal structure of the $tRNA^{Ala}$ acceptor stem (28). Taking into account that four hydroxyl groups were inner-sphere ligands of this Sr^{2+} ion, whereas inner-sphere coordination of 2′-OH ligands to Mg^{2+} seems to be rare (29), it is an intriguing possibility that Sr^{2+} fails to support M1 RNA catalysis owing to inner-sphere coordination to the 2′-OH at nt −1 of the substrate. A role for this substituent in Sr^{2+} binding is indeed indicated by a weaker inhibitory effect of Sr^{2+} in the context of the ptRNA substrate with a 2′-F modification at nt −1 (Figure 7, see Discussion).

Further information on binding of Sr^{2+} to RNA stems from high-resolution structures of the leadzyme in the presence of Mg^{2+} versus Mg^{2+} plus Sr^{2+} (30). Three Mg^{2+} and three Sr^{2+} ions were identified, the Sr^{2+} ions occupying different sites on the RNA than the Mg^{2+} ions. All three Mg^{2+} ions contacted the RNA duplex via their canonical octahedral hexa-hydration sphere, while ligand spheres of the three Sr^{2+} ions varied in number and did not uniformly consist of inner-shell water molecules. One Sr^{2+} ion ([Sr]3,(30)) had three water molecules, three inner-sphere base or phosphate oxygen ligands, and was 3.8 Å from the oxygen of the 2′-OH at C23 that serves as the nucleophile in the leadzyme reaction after proton abstraction by catalytic Pb^{2+}. Sr^{2+} coordination next to the 2′-OH of C23 offered an explanation why Sr^{2+} inhibits catalysis by Pb^{2+} (30). The same Sr^{2+} ion also caused modest but significant local changes in the immediate vicinity of the cleavage site, thereby favoring a 'pre-catalytic' over the 'ground-state' conformation of the leadzyme. Such local, Sr^{2+}-induced changes in the active site of RNase P RNA–substrate complexes may well have contributed to the inhibition effects seen in the RNase P system.

Effects of Sr^{2+} and Zn^{2+} on substrate binding and structure

K_d measurements (Figure 3A and Table 1) were performed with trace amounts of ^{32}P-labeled ptRNA and varying excess amounts of enzyme using a gel filtration spin column assay (8,23). Zn^{2+} increased the proportion of binding-deficient ptRNA molecules at saturating enzyme concentration (i.e. at the endpoint), a feature that is attributable to Zn^{2+} ions bound to ptRNA. Increasing Sr^{2+} concentrations at constant 20 mM Zn^{2+} largely reduced this binding-deficient ptRNA fraction, suggesting that Sr^{2+} can displace many of the deleterious Zn^{2+} ions from the substrate. The presence of 20 mM Zn^{2+} also caused a constant 2–3-fold increase in K_d over the entire range of tested Sr^{2+} concentrations (5–80 mM, Figure 3A). This indicates that Sr^{2+} is unable to displace Zn^{2+} (or to compensate its deleterious effects) at some sites where Zn^{2+} directly or indirectly impairs high-affinity substrate binding. Since K_d reflects structural properties of enzyme and substrate, the Zn^{2+} binding sites responsible for this K_d increase may be on the substrate and/or enzyme. To understand the structural effects of Zn^{2+} observed in the present study, it is instructive to inspect the Zn^{2+} binding sites detected in yeast $tRNA^{Phe}$ crystals (31). Five bound Zn^{2+} ions were identified, two of which, Zn(1) and Zn(2), replaced tightly bound Mg^{2+} ions in the U8–U12 region and in the D loop [corresponding to the Mg^{2+} binding sites 1 and 3 in Jovine *et al*. (32)], one [Zn(3)] overlapping with the weak Mg^{2+} binding site 7 in (32), and the remaining two [Zn(4,5)] being Zn^{2+}-specific or transition metal ion-specific sites in base-paired regions. All five Zn^{2+} ions were coordinated tetrahedrally, and four of them were bound by direct coordination to a guanine N7 at positions where the G residue is flanked by a purine residue on its 5′ side. Zn(1) is shifted ~2 Å relative to Mg^{2+} at this site. Based on these observations, Zn^{2+} may well cause specific changes of tRNA conformation or may occupy novel Zn^{2+}-specific sites that disturb ptRNA interaction with M1 RNA. The preference of Zn^{2+} for purine–guanine dinucleotides also in paired regions implies that (i) some Zn^{2+} binding sites may directly perturb E·S contacts involving acceptor and T stems regions and (ii) that effects of Zn^{2+} will be to some extent sequence-specific and thus specific for every individual RNA under investigation.

Effects of $Co(NH_3)_6^{3+}$ on M1 RNA-catalyzed cleavage

The addition of 5 mM $Co(NH_3)_6^{3+}$ to 20 mM Zn^{2+} stimulated ptRNA turnover ~2-fold, but higher $Co(NH_3)_6^{3+}$ concentrations were inhibitory as observed for Sr^{2+} (Figure 2C and D). Recently, inhibition of the *B.subtilis* RNase P holoenzyme by $Co(NH_3)_6^{3+}$ with Mg^{2+} as the catalytic cofactor (9) was discussed to indicate that $Co(NH_3)_6^{3+}$ displaces a metal ion for which the ionization or the displacement of a water molecule from the metal hydration shell is required. Here, it is instructive to compare the properties of Sr^{2+} and $Co(NH_3)_6^{3+}$, which showed similar inhibition effects (Figure 2C and D). Since water ligands can dissociate from the hydration shell of Sr^{2+} (28) but ammine ligands do not dissociate from the inert octahedral complex cation $[Co(NH_3)_6^{3+}]$ (33), the remaining common feature of the two is the low degree of ionization of water ligands at pH ⩽ 7 [pK_a of Sr^{2+} aqua ion = 13.2; (27)] in the case of Sr^{2+} and the complete absence of ionizable water ligands in the case of $Co(NH_3)_6^{3+}$. This would be consistent with the involvement of a $Me[H_2O]_5[OH]^+$ species in the catalytic process (9,15,24).

Effects of $Co(NH_3)_6^{3+}$ on substrate structure and binding

Soaking of yeast $tRNA^{Gly}$ crystals with $Co(NH_3)_6Cl_3$ identified three $[Co(NH_3)_6]^{3+}$ complexes which, however, did not replace strongly bound Mg^{2+} ions (34). Two bound to double-helical guanylguanosine sequences (G3/G4 [Co(2)] and G42/G43 [Co(1)]) and the third [Co(3)] to the purine–purine sequence A44/G45, in all cases in the major groove via hydrogen bonding of *cis*-ammine ligands to the N7 and O6 functions of adjacent purine bases. Additional hydrogen bonding occurred to O4 of U residues and to phosphate oxygens, but no direct metal–nucleotide bonds were observed (34). Interestingly, the binding site for Zn(5) [see above; (31)] overlapped with the site for Co(1), both contacting the N7 and O6 functions of G42 and G43. However, coordination of the tetrahedral Zn(5) involved an innersphere contact to the N7 of G43, and the octahedral Co(1) formed two additional contacts to non-bridging phosphate oxygens at positions 24 and 42 (34).

We observed that only about one-fourth of the ptRNA molecules were capable of binding to M1 RNA at saturating enzyme concentrations in the presence of 80 mM $Co(NH_3)_6^{3+}$

compared with the conditions of 80 mM Sr^{2+} (Table 1). One explanation may be related to the preference of $Co(NH_3)_6^{3+}$ for GG dinucleotides in paired regions (see above) and the multiple presence of such potential binding sites in our ptRNA^{Gly} (Figure 1). Binding of $Co(NH_3)_6^{3+}$ to some sites in the acceptor stem and T arm may prevent crucial contacts to M1 RNA either directly or may perturb the tRNA tertiary fold.

ACKNOWLEDGEMENTS

We thank Dagmar K. Willkomm for critical reading of the manuscript, Sybille Siedler and Dominik Helmecke for excellent technical assistance, and Michael Weber for the design of Figure 5. Financial support for these studies from the Deutsche Forschungsgemeinschaft (HA 1672/7-3/7-4) is acknowledged. Funding to pay the Open Access publication charges for this article was provided by the Fonds der Chemischen Industrie.

Conflict of interest statement. None declared.

REFERENCES

1. Frank,D.N. and Pace,N.R. (1998) Ribonuclease P: unity and diversity in a tRNA processing ribozyme. *Annu. Rev. Biochem.*, **67**, 153–180.
2. Altman,S. and Kirsebom,L.A. (1999) Ribonuclease P. In Gesteland,R.F., Cech,T. and Atkins,J.F. (eds), *The RNA World, 2nd edn*. Cold Spring Harbor Laboratory Press, Cold Spring Harbor, NY, pp. 351–380.
3. Schön,A. (1999) Ribonuclease P: the diversity of a ubiquitous RNA processing enzyme. *FEMS Microbiol. Rev.*, **23**, 391–406.
4. Guerrier-Takada,C., Gardiner,K., Marsh,T., Pace,N. and Altman,S. (1983) The RNA moiety of ribonuclease P is the catalytic subunit of the enzyme. *Cell*, **35**, 849–857.
5. Brown,J.W. (1998) The ribonuclease P database. *Nucleic Acids Res.*, **26**, 351–352.
6. Smith,D. and Pace,N.R. (1993) Multiple magnesium ions in the ribonuclease P reaction mechanism. *Biochemistry*, **32**, 5273–5281.
7. Warnecke,J.M., Fürste,J.P., Hardt,W.-D., Erdmann,V.A. and Hartmann,R.K. (1996) Ribonuclease P (RNase P) RNA is converted to a Cd^{2+}-ribozyme by a single Rp-phosphorothioate modification in the precursor tRNA at the RNase P cleavage site. *Proc. Natl Acad. Sci. USA*, **93**, 8924–8928.
8. Warnecke,J.M., Held,R., Busch,S. and Hartmann,R.K. (1999) Role of metal ions in the hydrolysis reaction catalyzed by RNase P RNA from *Bacillus subtilis*. *J. Mol. Biol.*, **290**, 433–445.
9. Kurz,J.C. and Fierke,C.A. (2002) The affinity of magnesium binding sites in the *Bacillus subtilis* RNase P × pre-tRNA complex is enhanced by the protein subunit. *Biochemistry*, **41**, 9545–9558.
10. Kufel,J. and Kirsebom,L.A. (1998) The P15-loop of *Escherichia coli* RNase P RNA is an autonomous divalent metal ion binding domain. *RNA*, **4**, 777–788.
11. Brännvall,M. and Kirsebom,L.A. (2001) Metal ion cooperativity in ribozyme cleavage of RNA. *Proc. Natl Acad. Sci. USA*, **98**, 12943–12947.
12. Brännvall,M., Pettersson,F. and Kirsebom,L.A. (2002) The residue immediately upstream of the RNase P cleavage site is a positive determinant. *Biochimie*, **84**, 693–703.
13. Christian,E.L., Kaye,N.M. and Harris,M.E. (2002) Evidence for a polynuclear metal ion binding site in the catalytic domain of ribonuclease P RNA. *EMBO J.*, **21**, 2253–2262.
14. Smith,D., Burgin,A.B., Haas,E.S. and Pace,N.R. (1992) Influence of metal ions on the ribonuclease P reaction. Distinguishing substrate binding from catalysis. *J. Biol. Chem.*, **267**, 2429–2436.
15. Guerrier-Takada,C., Haydock,K., Allen,L. and Altman,S. (1986) Metal ion requirements and other aspects of the reaction catalyzed by M1 RNA, the RNA subunit of ribonuclease P from *Escherichia coli*. *Biochemistry*, **25**, 1509–1515.
16. Kazakov,S. and Altman,S. (1991) Site-specific cleavage by metal ion cofactors and inhibitors of M1 RNA, the catalytic subunit of RNase P from *Escherichia coli*. *Proc. Natl Acad. Sci. USA*, **88**, 9193–9197.
17. Brännvall,M., Mikkelsen,N.E. and Kirsebom,L.A. (2001) Monitoring the structure of *Escherichia coli* RNase P RNA in the presence of various divalent metal ions. *Nucleic Acids Res.*, **29**, 1426–1432.
18. Perreault,J.P. and Altman,S. (1992) Important 2′-hydroxyl groups in model substrates for M1 RNA, the catalytic RNA subunit of RNase P from *Escherichia coli*. *J. Mol. Biol.*, **226**, 399–409.
19. Perreault,J.P. and Altman,S. (1993) Pathway of activation by magnesium ions of substrates for the catalytic subunit of RNase P from *Escherichia coli*. *J. Mol. Biol.*, **230**, 750–756.
20. Persson,T., Cuzic,S. and Hartmann,R.K. (2003) Catalysis by RNase P RNA: unique features and unprecedented active site plasticity. *J. Biol. Chem.*, **278**, 43394–43401.
21. Zuleeg,T., Hartmann,R.K., Kreutzer,R. and Limmer,S. (2001) NMR spectroscopic evidence for $Mn^{2+}(Mg^{2+})$ binding to a precursor-tRNA microhelix near the potential RNase P cleavage site. *J. Mol. Biol.*, **305**, 181–189.
22. Busch,S., Kirsebom,L.A., Notbohm,H. and Hartmann,R.K. (2000) Differential role of the intermolecular base-pairs G292-C_{75} and G293-C_{74} in the reaction catalyzed by *Escherichia coli* RNase P RNA. *J. Mol. Biol.*, **299**, 941–951.
23. Beebe,J.A. and Fierke,C.A. (1994) A kinetic mechanism for cleavage of precursor tRNA^{Asp} catalyzed by the RNA component of *Bacillus subtilis* ribonuclease P. *Biochemistry*, **33**, 10294–10304.
24. Chen,Y., Li,X. and Gegenheimer,P. (1997) Ribonuclease P catalysis requires Mg^{2+} coordinated to the *pro-*R_P oxygen of the scissile bond. *Biochemistry*, **36**, 2425–2438.
25. Kuimelis,R.G. and McLaughlin,L.W. (1998) Mechanisms of ribozyme-mediated RNA cleavage. *Chem. Rev.*, **98**, 1027–1044.
26. Cotton,F.A. and Wilkinson,G. (1988) *Advanced Inorganic Chemistry, 5th edn*. John Wiley & Sons, NY, Chichester, Brisbane, Toronto, Singapore.
27. Feig,A.L. and Uhlenbeck,O.C. (1999) The role of metal ions in RNA biochemistry. In Gesteland,R.F., Cech,T. and Atkins,J.F. (eds), *The RNA World, 2nd edn*. John Wiley & Sons, NY, Chichester, Brisbane, Toronto, Singapore. Cold Spring Harbor Laboratory Press, Cold Spring Harbor, NY, pp. 287–319.
28. Mueller,U., Schübel,H., Sprinzl,M. and Heinemann,U. (1999) Crystal structure of acceptor stem of tRNA^{Ala} from *Escherichia coli* shows unique G·U wobble base pair at 1.16 Å resolution. *RNA*, **5**, 670–677.
29. Juneau,K., Podell,E., Harrington,D.J. and Cech,T. (2001) Structural basis of the enhanced stability of a mutant ribozyme domain and a detailed view of RNA–solvent interactions. *Structure*, **9**, 221–231.
30. Wedekind,J.E. and McKay,D.B. (2003) Crystal structure of the leadzyme at 1.8 Å resolution: metal ion binding and the implications for catalytic mechanism and allo site ion regulation. *Biochemistry*, **42**, 9554–9563.
31. Rubin,J.R., Wang,J. and Sundaralingam,M. (1983) X-ray diffraction study of the zinc(II) binding sites in yeast phenylalanine transfer RNA. Preferential binding of zinc to guanines in purine–purine sequences. *Biochim. Biophys. Acta*, **756**, 111–118.
32. Jovine,L., Djordjevic,S. and Rhodes,D. (2000) The crystal structure of yeast phenylalanine tRNA at 2.0 Å resolution: cleavage by Mg^{2+} in 15-year old crystals. *J. Mol. Biol.*, **301**, 401–414.
33. Cowan,J.A. (1993) Metallobiochemistry of RNA. $Co(NH_3)_6^{3+}$ as a probe for Mg2 (aq) binding sites. *J. Inorg. Biochem.*, **49**, 171–175.
34. Hingerty,B.E., Brown,R.S. and Klug,A. (1982) Stabilization of the tertiary structure of yeast phenylalanine tRNA by $[Co(NH_3)_6]^{3+}$. X-ray evidence for hydrogen bonding to pairs of guanine bases in the major groove. *Biochim. Biophys. Acta*, **697**, 78–82.
35. Warnecke,J.M., Sontheimer,E.J., Piccirilli,J.A. and Hartmann,R.K. (2000) Active site constraints in the hydrolysis reaction catalyzed by bacterial RNase P: analysis of precursor tRNAs with a single 3′-*S*-phosphorothiolate internucleotide linkage. *Nucleic Acids Res.*, **28**, 720–727.
36. Zuleeg,T., Hansen,A., Pfeiffer,T., Schubel,H., Kreutzer,R., Hartmann,R.K. and Limmer,S. (2001) Correlation between processing efficiency for ribonuclease P minimal substrates and conformation of the nucleotide −1 at the cleavage position. *Biochemistry*, **40**, 3363–3369.
37. Zuleeg,T., Hartmann,R.K., Kreutzer,R. and Limmer,S. (2001) NMR spectroscopic evidence for Mn^{2+} (Mg^{2+}) binding to a *precursor*-tRNA microhelix near the potential RNase P cleavage site. *J. Mol. Biol.*, **305**, 181–189.